J|A|C|S
ARTICLES
Published on Web 12/09/2005

Models for the Molybdenum Hydroxylases: Synthesis, Characterization and Reactivity of *cis*-Oxosulfido-Mo(VI) Complexes

Christian J. Doonan,[†,§] David J. Nielsen,[†] Paul D. Smith,[†,||] Jonathan M. White,[†] Graham N. George,[‡,§] and Charles G. Young*[,†]

Contribution from the School of Chemistry, University of Melbourne, Victoria 3010, Australia, and Stanford Synchrotron Radiation Laboratory, SLAC, Stanford University, P.O. Box 4349, MS 69, Stanford, California 94309

Received September 5, 2005; E-mail: cgyoung@unimelb.edu.au

Abstract: Atom transfer reactions have been employed to convert $Tp^{iPr}MoO_2(OAr)$ into monomeric *cis*-oxosulfido-Mo(VI) and dimeric μ-disulfido-Mo(V) species, $[Tp^{iPr}MoOS(OAr)]_n$ (Tp^{iPr} = hydrotris(3-isopropylpyrazol-1-yl)borate; OAr = phenolate or naphtholate derivative; n = 1 and 2, respectively). Dark red, monomeric $Tp^{iPr}MoOS(OAr)$ complexes contain distorted octahedral *cis*-oxosulfido-Mo(VI) centers, with d(Mo=O) = 1.692(5) Å, d(Mo=S) = 2.132(2) Å, and $\angle$(O=Mo=S) = 103.68(16)° for the 2-*sec*-butylphenolate derivative. Dark red-purple, dimeric $[Tp^{iPr}MoOS(OAr)]_2$ complexes undergo S−S bond cleavage forming monomeric oxosulfido-Mo(VI) species in solution. In the solid state, the 3,5-di-*tert*-butylphenolate derivative exhibits a centrosymmetric structure, with distorted octahedral anti oxo-Mo(V) centers bridged by a disulfido-$\kappa S,\kappa S'$ ligand. Hydrolysis of the oxosulfido-Mo(VI) complexes results in the formation of $[Tp^{iPr}MoO]_2(\mu\text{-}S_2)(\mu\text{-}O)$. In anaerobic solutions, certain oxosulfido-Mo(VI) complexes convert to molybdenyl complexes bearing bidentate 2-mercaptophenolate or related naphtholate ligands formed via intramolecular attack of the sulfido ligand on a coligand C−H group. The oxosulfido-Mo(VI) complexes serve as precursors to biologically relevant Mo(V) and heterobimetallic MoO(μ-S)Cu species and undergo a range of biomimetic reactions.

Introduction

Molybdenum, an ultratrace element required by all eukaryotic and most prokaryotic organisms, is present in over fifty pterin-containing redox enzymes falling into three recognized families.[1−5] Members of the dimethyl sulfoxide reductase and sulfite oxidase families catalyze key reactions in nitrogen assimilation, amino acid catabolism, detoxification, and respiration. Members of the xanthine oxidase (Mo hydroxylase) family are responsible for carbon-centered reactions in purine catabolism, hormone and retinoic acid synthesis, drug metabolism, prodrug activation, detoxification, and oxidative stress response. Most of these reactions involve hydroxylation (C−H → C−OH, using water as the source of oxygen), dehydroxylation, or transhydroxylation of substrates. In humans, deficiency or dysfunction of xanthine oxidase is associated with diseases such as xanthinuria, hyperuricemia, and gout and with free-radical tissue damage associated with postischemic reperfusion injury, arthritis, atherosclerosis, and Alzheimer's and Parkinson's diseases.[1−6] The proper function of Mo enzymes is also important in agriculture, animal science, and environmental science and in global cycles and meteorological phenomena.[1−5]

The oxidized active sites of Mo hydroxylases generally contain a square pyramidal $[(MPT)Mo^{VI}OS(OH)]^-$ (MPT = molybdopterin derivative) center bearing a catalytically essential terminal sulfido ligand.[1−5] Recent studies[7,8] have provided strong support for the presence of an apical oxo ligand and equatorial sulfido and hydroxo (rather than aqua) ligands at the Mo site of xanthine oxidase. In one Mo hydroxylase, i.e., the novel carbon monoxide dehydrogenase from the aerobic eubacterium *Oligotropha carboxidovorans*, the sulfido ligand acts as a bridge to a Cu(cysteine) moiety.[9] Despite considerable progress in the structural[10] and mechanistic[1] description of these enzymes, the

[†] University of Melbourne.
[‡] Stanford University.
[§] Present address: Department of Geological Sciences, University of Saskatchewan, 114 Science Place, Saskatoon SK, S7N 5E2, Canada.
[||] Present address: Department of Chemistry & Materials, The Manchester Metropolitan University, John Dalton Building, Chester Street, Manchester M1 5GD, U.K.

(1) Hille, R. *Chem. Rev.* **1996**, *96*, 2757−2816.
(2) Pilato, R. S.; Stiefel, E. I. In *Bioinorganic Catalysis*, 2nd ed.; Reedijk, J., Bouwman, E., Eds.; Marcel Dekker: New York, 1999; pp 81−152.
(3) Sigel, A., Sigel, H., Eds. *Metal Ions in Biological Systems*; Marcel Dekker: New York, 2002; Vol. 39.
(4) Tunney, J. M.; McMaster, J.; Garner, C. D. In *Comprehensive Coordination Chemistry II*; McCleverty, J. A., Meyer, T. J., Eds.; Elsevier Pergamon: Amsterdam, 2004; Vol. 8, Chapter 8.18, pp 459−477.
(5) Young, C. G. In *Encyclopedia of Inorganic Chemistry 2*; King, R. B., Ed.; Wiley: Chichester, UK, 2005; Vol. V, pp 3321−3340.
(6) Harrison, R. *Free Radical Biol. Med.* **2002**, *33*, 774−797.
(7) Okamoto, K.; Matsumoto, K.; Hille, R.; Eger, B. T.; Pai, E. F.; Nishino, T. *Proc. Natl. Acad. Sci. U.S.A.* **2004**, *101*, 7931−7936.
(8) Doonan, C. J.; Stockert, A.; Hille, R.; George, G. N. *J. Am. Chem. Soc.* **2005**, *127*, 4518−4522.
(9) Dobbek, H.; Gremer, L.; Kiefersauer, R.; Huber, R.; Meyer, O. *Proc. Natl. Acad. Sci. U.S.A.* **2002**, *99*, 15971−15976.
(10) Dobbek, H.; Huber, R. In *Metal Ions in Biological Systems*; Sigel, A., Sigel, H., Eds.; Marcel Dekker: New York, 2002; Vol. 39, pp 227−263.

Scheme 1. Synthesis and Reactions of $Tp^{iPr}MoOS(OAr)$ Complexes

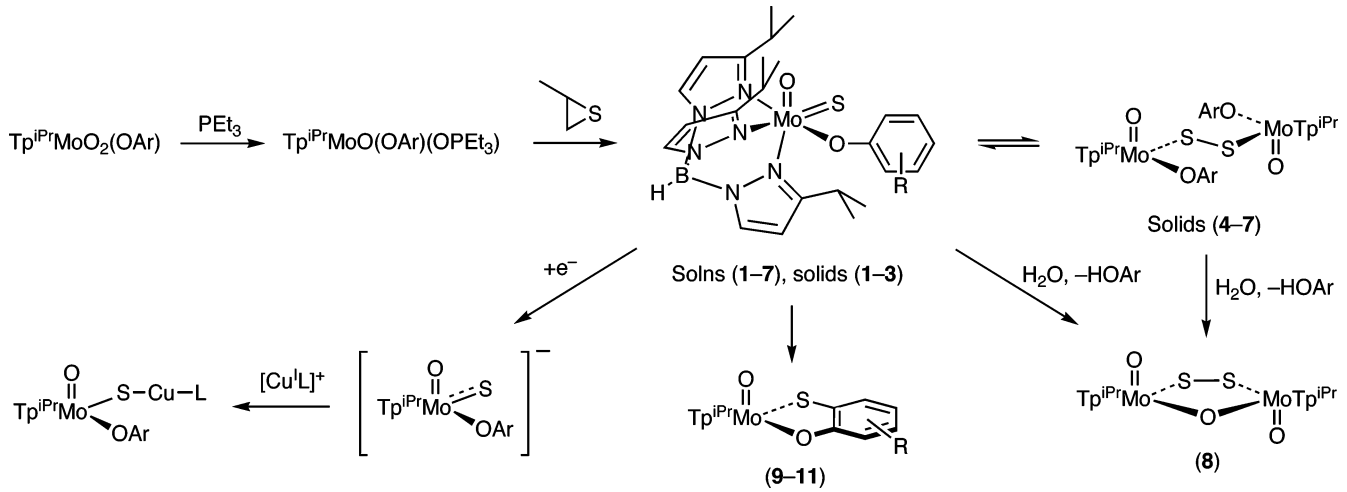

fundamental chemical and electronic properties of $[MoOS]^{n+}$ centers are poorly understood; consequently, their impact on enzyme behavior is difficult to assess. This is primarily due to the scarcity of oxosulfido-Mo(VI) and -Mo(V) complexes[11,12] and the complete lack of MoO(μ-S)Cu species. However, the documented properties of $[MoOS]^{n+}$ complexes suggest the importance of Mo/S-based frontier orbitals to their behavior and, by inference, that of Mo hydroxylases.[11] Thus, structural, spectroscopic, and chemical investigations of oxosulfido- and hydrosulfido-Mo(VI−IV) complexes are fundamentally important for a complete understanding of the key centers and orbital control of reactivity in Mo hydroxylases.

For many years, mononuclear oxosulfido-Mo(VI) complexes were restricted to tetrahedral thiomolybdates and pseudo-tetrahedral cyclopentadienyl and dialkylhydroxylamido complexes; related Mo(V) and Mo(IV) complexes and clean biomimetic reactions, e.g., cyanolysis, are not observed for such complexes.[11,12] More recently, Thapper et al. reported the synthesis of $MoOS(OSiPh_3)_2L$ (L = bpy or phen derivative) from the reactions of $K_2[MoO_3S]$, $ClSiPh_3$, and L in basic (NEt_3) acetonitrile.[13] The presence of monomers containing unperturbed, terminal sulfido ligands was established by crystallographic and EXAFS studies. Reduced counterparts and biomimetic reactions have not been reported for complexes of this type.

The oxosulfido-Mo(VI) complexes, $Tp^*MoOS(S_2PR_2)$ (R = ^{i}Pr, Ph; Tp* = hydrotris(3,5-dimethylpyrazol-1-yl)borate), contain a π-bonded sulfido ligand (d(Mo=S) = 2.21 Å) stabilized by a weak, intramolecular S···S interaction (d(S···S) = 2.39 Å) involving the monodentate dithiophosphinate ligand.[14] They are formed by sulfur atom transfer from propylene sulfide to $Tp^*MoO(S_2PR_2)$, are amenable to reduction to biologically relevant oxosulfido- and oxo(hydrosulfido)-Mo(V) species, and participate in clean biomimetic reactions, e.g., cyanolysis and regeneration by sulfide.[14] Underscoring the redox versatility of Mo/S units, the complexes also undergo both direct reduction or induced internal reduction (net oxidation) to produce oxo-Mo(V) species.[15] Related hydro(5-isopropylpyrazol-1-yl)bis(3-isopropylpyrazol-1-yl)borate complexes are also known.[16]

Subsequently, an unperturbed oxosulfido-Mo(VI) complex, $Tp^{iPr}MoOS(OPh)$, was prepared in situ and isolated as the μ-disulfido-Mo(V) dimer, $[Tp^{iPr}MoO(OPh)]_2(\mu\text{-}S_2)$ (Tp^{iPr} = hydrotris(3-isopropylpyrazol-1-yl)borate);[17] the structural, spectroscopic, and chemical properties of the material were consistent with a delicately poised monomer−dimer equilibrium. Our desire to produce *strictly* monomeric oxosulfido-Mo(VI) complexes and to extend synthetic hydroxylase models to reduced states and biomimetic reactions has led to further investigation of this promising system. The investigation began with systematic electrochemical and structural studies of dioxo-Mo(VI) complexes and the identification of precursors for stable, monomeric oxosulfido-Mo(VI) complexes.[18,19] Synthetically important oxygen atom transfer reactions were then surveyed, and the immediate precursors to the title complexes, viz., novel oxo(phosphine oxide)-Mo(IV) species, were isolated and characterized.[19,20] Finally, a systematic study of the reactions of these complexes with sulfur atom donors yielded the desired oxosulfido-Mo(VI) species.

We report here the synthesis and spectroscopic and structural characterization of $[Tp^{iPr}MoOS(OAr)]_n$ (n = 1, 2; OAr = alkyl substituted phenolate or naphtholate derivative) and the "downstream" derivatives (thermodynamic products) in Scheme 1. The isolation of *strictly* monomeric oxosulfido-Mo(VI) complexes (when OAr = $OC_6H_4{}^s$Bu-2 (**1**), $OC_6H_4{}^t$Bu-2 (**2**), OC_6H_4Ph-4 (**3**)), additional examples of monomer−dimer equilibria (when OAr = $OC_6H_4{}^t$Bu-3 (**4**), $OC_6H_3{}^t$Bu$_2$-3,5 (**5**), OC_6H_4Ph-3 (**6**), OPh (**7**)[17]), the characterization of the thermodynamic product in the (**1**−**7**)/water system, viz., $[Tp^{iPr}MoO]_2(\mu\text{-}S_2)(\mu\text{-}O)$ (**8**), and the identification of an unprecedented reaction between Mo=S and aromatic C−H groups are documented. The presence of monomeric, unperturbed oxosulfido-Mo(VI) centers has been

(11) Young, C. G. *J. Biol. Inorg. Chem.* **1997**, *2*, 810−816.
(12) Young, C. G. In *Comprehensive Coordination Chemistry II*; McCleverty, J. A., Meyer, T. J., Eds.; Elsevier Pergamon: Amsterdam, 2004; Vol. 4, Chapter 4.7, pp 415−527.
(13) Thapper, A.; Donahue, J. P.; Musgrave, K. B.; Willer, M. W.; Nordlander, E.; Hedman, B.; Hodgson, K. O.; Holm, R. H. *Inorg. Chem.* **1999**, *38*, 4104−4114.
(14) (a) Eagle, A. A.; Laughlin, L. J.; Young, C. G.; Tiekink, E. R. T. *J. Am. Chem. Soc.* **1992**, *114*, 9195−9197. (b) Laughlin, L. J. Ph.D. Dissertation, University of Melbourne, 1993.
(15) Hill, J. P.; Laughlin, L. J.; Gable, R. W.; Young, C. G. *Inorg. Chem.* **1996**, *35*, 3447−3448.
(16) Young, C. G.; Laughlin, L. J.; Colmanet, S.; Scrofani, S. D. B. *Inorg. Chem.* **1996**, *35*, 5368−5377.
(17) Smith, P. D.; Slizys, D. A.; George, G. N.; Young, C. G. *J. Am. Chem. Soc.* **2000**, *122*, 2946−2947.
(18) Millar, A. J.; Doonan, C. J.; Laughlin, L. J.; Tiekink, E. R. T.; Young, C. G. *Inorg. Chim. Acta* **2002**, *337*, 393−406.
(19) Doonan, C. J.; Millar, A. J.; Nielsen, D. J.; Young, C. G. *Inorg. Chem.* **2005**, *44*, 4506−4514.
(20) Millar, A. J.; Doonan, C. J.; Smith, P. D.; Nemykin, V. N.; Basu, P.; Young, C. G. *Chem.−Eur. J.* **2005**, *11*, 3255−3267.

confirmed by the crystal structures of **1**−**3**, the structure of **1** being the first nondisordered structure of an octahedral, oxosulfido-Mo(VI) complex. The crystal structures of **5** and **8** reveal metal centers linked by μ-disulfido and μ-disulfido-μ-oxo bridges, respectively. Finally and quite remarkably, the sulfido ligand in several of the complexes has been observed to attack a coligand aromatic C−H group, to generate molybdenyl complexes bearing bidentate 2-mercaptophenolate(2−) or related naphtholate(2−) ligands, viz., Tp$^{i\mathrm{Pr}}$MoO(OSAr-1,2) (Ar = $C_6H_3{}^s$Bu-6 (**9**), $C_6H_3{}^t$Bu-4 (**10**), $C_{10}H_6$ (**11**)). The complexes have been characterized by spectroscopic methods, and the crystal structure of **11** has been determined. In addition, the oxosulfido-Mo(VI) complexes are amenable to electrochemical or chemical reductions providing access to authentic oxosulfido-Mo(V) complexes.[17] These, in turn, react with Cu(I) species to produce unprecedented models for the paramagnetic MoO-(μ-S)Cu site of CO dehydrogenase, e.g., Tp$^{i\mathrm{Pr}}$MoO(OAr)(μ-S)-Cu(Me$_3$tcn) (Me$_3$tcn = 1,4,7-trimethyl-1,4,7-triazacyclononane).[21] Accordingly, the oxosulfido-Mo(VI) complexes and reactions described here are significant advances toward a broad model of the Mo hydroxylases (Scheme 1). Moreover, advanced spectroscopic studies of the complexes have provided important insights into the electronic structure of $[MoOS]^{n+}$ (n = 1, 2) centers and related enzyme states.[22]

Experimental Section

Materials and Methods. Unless stated, all reactions, manipulations, and solution studies were performed under an atmosphere of dinitrogen using standard Schlenk and glovebox techniques and carefully dried and deoxygenated solvents and reagents. The precursors, Tp$^{i\mathrm{Pr}}$MoO(OAr)(OPEt$_3$),[19,20] and samples of **7**[17] were prepared according to literature methods. Anaerobic chromatographic separations were performed using Merck Art. 7734 Kieselgel 60 mesh dried at 120 °C for 24 h.

Infrared spectra were recorded on a Biorad FTS 165 FTIR spectrophotometer. Proton NMR spectra were obtained using a Varian UnityPlus 400 spectrometer and were referenced to internal $CHCl_3$ (δ_H 7.26). Mass spectra were recorded on a Bruker BioApex 47e FTMS fitted with an Analytica electrospray source operating with capillary voltages between 30 and 120 V. Shimadzu UV-240 and Hitachi 150-20 UV spectrophotometers were used to record electronic (UV−visible) spectra. EPR spectra were recorded on a Bruker FT ECS-106 spectrometer using 1,1-diphenyl-1,2-picrylhydrazyl as reference. Electrochemical experiments were performed on a Cypress Electrochemical System II using a 3 mm glassy-carbon working electrode and platinum auxiliary electrodes. The reference electrode consisted of an $Ag/AgNO_3$ (0.01 M in MeCN) electrode incorporated into a salt bridge containing supporting electrolyte to minimize Ag^+ leaching into solution. Samples were prepared in solutions of acetonitrile/0.2 M $NBu^n{}_4BF_4$, and scans were calibrated using ferrocene as internal reference. Potentials are reported relative to the Saturated Calomel Electrode (SCE). Microanalyses were performed by Atlantic Microlabs, Norcross, GA, and vapor pressure osmometry measurements (in CH_2Cl_2) by the Microanalytical Unit at the Research School of Chemistry, Australian National University. The spectroscopic properties of the compounds are summarized in Tables 1 and 2. Microanalytical data and full listings of IR data are included as Supporting Information.

Syntheses. Tp$^{i\mathrm{Pr}}$MoOS(OC$_6$H$_4{}^s$Bu-2) (1). Propylene sulfide (0.40 mL, 5.1 mmol) was added to a slurry of Tp$^{i\mathrm{Pr}}$MoO(OC$_6$H$_4{}^s$Bu-2)(OPEt$_3$) (750 mg, 1.02 mmol) in MeCN (4 mL), and the mixture was stirred; the precursor rapidly dissolved, and the reaction changed color from green through brown to dark red. The red precipitate that formed after 30 min was isolated by rapid filtration in air, washed (with 3 × 1 mL dry MeCN at −30 °C, then 2 mL of dry hexane), and vacuum-dried. Yield: 430 mg (67%).

Tp$^{i\mathrm{Pr}}$MoOS(OC$_6$H$_4{}^t$Bu-2) (2). Propylene sulfide (0.21 mL, 2.7 mmol) was added to a slurry of Tp$^{i\mathrm{Pr}}$MoO(OC$_6$H$_4{}^t$Bu-2)(OPEt$_3$) (200 mg, 0.27 mmol) in MeCN (4 mL), and the mixture was stirred for 1 h. The volume of the solution was then reduced in vacuo until crystallization commenced. After cooling at −30 °C for a further 30 min, the crystals were isolated by filtration, washed with cold MeCN, and dried in vacuo. Yield: 80 mg (47%).

Tp$^{i\mathrm{Pr}}$MoOS(OC$_6$H$_4$Ph-4) (3). Propylene sulfide (1.10 mL, 14 mmol) was added to a solution of Tp$^{i\mathrm{Pr}}$MoO(OC$_6$H$_4$Ph-4)(OPEt$_3$) (2.07 g, 2.74 mmol) in MeCN (35 mL), and the mixture stirred overnight. The reaction was then worked up as described above for **2**. The dark red compound was isolated by filtration, washed with 3 × 1 mL of dry MeCN, and dried in vacuo. Yield: 1.25 g (70%).

[Tp$^{i\mathrm{Pr}}$MoO(OC$_6$H$_4{}^t$Bu-3)]$_2$(μ-S$_2$) (4). Method 1: Propylene sulfide (0.63 mL, 8.01 mmol) was added to a solution of Tp$^{i\mathrm{Pr}}$MoO(OC$_6$H$_4{}^t$Bu-3)(OPEt$_3$) (600 mg, 0.81 mmol) in MeCN (30 mL), and the mixture was stirred at 25−30 °C for 10 h. The reaction mixture was reduced to dryness and then reconstituted with 3:2 CH_2Cl_2/hexanes and chromatographed on silica gel using the same solvent as eluent. The first, major, red-brown band was collected, and the solution was reduced in volume to 5 mL and cooled to −30 °C overnight. The resultant dark red-purple microcrystalline solid was filtered and washed with cold hexanes and dried in vacuo. Yield: 250 mg (48%).

Method 2: Triethylphosphine (0.28 mL, 1.9 mmol) was added to a solution of Tp$^{i\mathrm{Pr}}$MoO$_2$(OC$_6$H$_4{}^t$Bu-3) (789 mg, 1.28 mmol) in dry MeCN (30 mL), and the mixture was allowed to stir overnight. Propylene sulfide (1.0 mL, 13 mmol) was then added via syringe to the resultant green solution, and the mixture was stirred for a further 3 h. Volume reduction to ca. 10 mL in vacuo and storage overnight at −30 °C yielded dark red-purple microcrystals. The product was isolated by filtration, washed with 3 × 1 mL portions of dry MeCN, and dried in vacuo. Yield: 521 mg (64%).

[Tp$^{i\mathrm{Pr}}$MoO(OC$_6$H$_3{}^t$Bu$_2$-3,5)]$_2$(μ-S$_2$) (5). The compound was prepared by a procedure analogous to Method 1 for **4**. The reaction mixture was stirred at 25−30 °C for 2−3 h and then worked up as described above. Yield: 345 mg (63%).

[Tp$^{i\mathrm{Pr}}$MoO(OC$_6$H$_4$Ph-3)]$_2$(μ-S$_2$) (6). Propylene sulfide (0.060 mL, 0.77 mmol) was added to a solution of Tp$^{i\mathrm{Pr}}$MoO(OC$_6$H$_4$Ph-3)(OPEt$_3$) (102 mg, 0.135 mmol) in MeCN (0.5 mL), and the mixture was stirred at 25−30 °C for 2 h. The resulting suspension was stored overnight at −30 °C, and the red-black product was filtered, washed with dry MeCN (3 × 0.5 mL at −30 °C), and dried in vacuo. Yield: 39 mg (44%).

[Tp$^{i\mathrm{Pr}}$MoO]$_2$(μ-S$_2$)(μ-O) (8). The brown-purple complex was obtained when the Tp$^{i\mathrm{Pr}}$MoOS(OAr) complexes were column chromatographed (as above) in air using reagent grade solvents. The addition of water to solutions containing Tp$^{i\mathrm{Pr}}$MoOS(OAr) also resulted in the isolation of crystals of **8** upon standing.

Tp$^{i\mathrm{Pr}}$MoO(OSC$_6$H$_3{}^s$Bu-6) (9). Propylene sulfide (0.20 mL, 2.6 mmol) was added to a solution of Tp$^{i\mathrm{Pr}}$MoO(OC$_6$H$_4{}^s$Bu-2)(OPEt$_3$) (200 mg, 0.272 mmol) in MeCN (30 mL), and the mixture stirred for 24 h. The mixture was then reduced to dryness, reconstituted with 1:1 CH_2Cl_2/hexanes, and column chromatographed on a silica gel column using 1:1 CH_2Cl_2/hexanes as eluent. The main brown fraction was collected and recrystallized from CH_2Cl_2−methanol. Yield: 65 mg (38%).

Tp$^{i\mathrm{Pr}}$MoO(OSC$_6$H$_3{}^t$Bu-4) (10). The reaction was performed and worked up as described above for **9** except that a reaction time of 12 h was employed. Yield: 80 mg (47%).

Tp$^{i\mathrm{Pr}}$MoO(OSC$_{10}$H$_6$) (11). The reaction was performed and worked up as described above for **9** except that a reaction time of 12 h was employed. Yield: 75 mg (43%).

(21) Gourlay, C.; Nielsen, D. J.; White, J. M.; Knottenbelt, S. Z.; Kirk, M. L.; Young, C. G. *J. Am. Chem. Soc.*, submitted for publication.
(22) Rubie, N. R.; Peariso, K.; Doonan, C. J.; George, G. N.; Young, C. G.; Kirk, M. L. *J. Am. Chem. Soc.* submitted for publication.

Table 1. Characterization Data for Diamagnetic Complexes

compd	*m/z* [M + H]$^+$	IR spectrum (cm^{-1})[a] ν(BH)	ν(MoO)	ν(MoS)	^{1}H NMR spectrum, δ (multiplicity, no. of H), in $CDCl_3$ Tp^{iPr} methyl[c]	Tp^{iPr} methine[d]	Tp^{iPr} ring[e]	OAr	λ_{max} (ϵ)[b]
Tp^{iPr}MoOS(OAr) (Ar, No.)									
$C_6H_4{}^s$Bu-2 (**1**)[f]	635	2495	902	485	–	–	–	–	503 (930), 410 (sh 2030)
$C_6H_4{}^t$Bu-2 (**2**)	635	2505	906	485	0.30, 0.46, 0.96, 1.23, 1.30, 1.31	3.15, 3.80, 4.84	5.87, 6.10, 6.19, 7.58, 7.70, 7.71	1.43 (s, 9H), 4.55 (d, 1H), 6.44 (t, 1H), 6.70 (t, 1H), 7.20 (d, 1H)	508 (800), 414 (sh 1830)
C_6H_4Ph-4 (**3**)	655	2487	915	484	0.92, 1.01, 1.21, 1.23, 1.26, 1.31	3.09, 3.72, 4.63	5.99, 6.17, 6.20, 7.56, 7.69 (2H)	7.19 (d, 2H), 7.31 (t, 1H), 7.43 (t, 2H), 7.59 (d, 2H), 7.63 (d, 2H)	540 (850), 419 (sh 1950)
$C_6H_4{}^t$Bu-3 (**4**)[g]	635	2513 (2496)	931 (913)	– (484)	0.84, 0.98, 1.12, 1.21, 1.25, 1.30	3.09, 3.73, 4.65	5.97, 6.16, 6.18, 7.53, 7.68 (2H)	1.27 (s, 9H), 6.91 (m, 1H), 7.04 (m, 2H), 7.30 (t, 1H)	514 (900), 408 (sh 2330)
$C_6H_3{}^t Bu_2$-3,5 (**5**)[g]	691	2499 (2496)	924 (913)	– (484)	0.76, 0.99, 1.03, 1.22, 1.27, 1.31	3.16, 3.80, 4.71	5.94, 6.16, 6.17, 7.52, 7.67 (2H)	1.28 (18H), 6.73 (2H), 7.02 (1H)	515 (730), 416 (sh 1570)
C_6H_4Ph-3 (**6**)[g]	655	2515 (2496)	941 (916)	– (484)	0.92, 1.00, 1.18, 1.23, 1.26, 1.31	3.13, 3.74, 4.63	5.98, 6.17, 6.20, 7.54, 7.68 (2H)	7.13 (dd, 1H), 7.1–7.4 (m, 3H), 7.41 (t, 1H), 7.45 (t, 2H), 7.64 (d, 2H)	515 (900), 415 (1700)
Ph (**7**)[g,h]	601[i]	2473	940 (914)	– (483)	0.88, 0.98, 1.17, 1.21, 1.25, 1.30	3.07, 3.70, 4.62	5.98, 6.16, 6.19, 7.54, 7.68, 7.68	7.01 (t, 1H), 7.13 (d, 2H), 7.33 (t, 2H)	503 (700), 402 (sh, 1090)
[Tp^{iPr}MoO]$_2$-(μ-S_2)(μ-O) (**8**)	984	2486	942	–	0.04, 0.71, 1.07, 1.16, 1.26, 1.37	2.75, 4.17, 4.62	5.93, 6.00, 6.20, 7.48, 7.56, 7.64	–	790 (125), 578 (600), 472 (sh 1700), 435 (2400)

[a] In KBr. For dimeric species (see footnote g), the values in parentheses were obtained from solution (CH_2Cl_2) spectra. [b] In $CHCl_3$, λ_{max} in nm, ϵ in M^{-1} cm^{-1}. [c] All doublet resonances integrating for 3H. [d] All septet resonances integrating for 1H each. [e] Unless indicated, all doublet resonances integrating for 1H each. [f] Complicated NMR spectrum due to presence of stereoisomers (see Supporting Information). [g] Monomeric in solution and dimeric in the solid state. [h] NMR in C_6D_6. See ref 17. [i] For [M + Na]$^+$.

Table 2. Characterization Data for Tp^{iPr}MoO(OSAr) Complexes

OSAr (no.)[a]	*m/z*[b]	ν(BH)	ν(Mo=O)	g_1	g_2	g_3	g_{iso}	A_{iso}[c]
$OSC_6H_3{}^s$Bu-6 (**9**)	634	2489	935	1.979	1.963	1.923	1.956	37.8
$OSC_6H_3{}^t$Bu-4 (**10**)	634	2488	942	1.979	1.963	1.928	1.956	38.0
$OSC_{10}H_6$ (**11**)	626	2507	933	1.979	1.963	1.925	1.955	37.3
Tp*MoO(OSC_6H_4)[d]	–	–	936	1.979	1.965	1.932	1.960	38.3

[a] Mercaptonaphtholato or 2-mercapto-*n*-alkylphenolato ligands and number of complex. [b] For [M + H]$^+$ ion. [c] In units of 10^{-4} cm^{-1}. [d] From ref 31.

X-ray Crystallography. Crystallographic data are summarized in Table 3. Unless stated, data were collected on a Bruker CCD area detector at 293 K using graphite monochromated Mo Kα radiation (0.710 73 Å) using 30 s frames over the range $2° < 2\theta < 50°$. Cell parameters were acquired by the SMART software package, and data reduction was performed with SAINT. Structures were solved by direct methods (SHELXS-97)[23] and refined using full-matrix least-squares refinement on F^2 (SHELXL-97).[24] Unless stated, all non-hydrogen atoms were found in difference electron density maps and refined anisotropically. Hydrogen atoms were included with fixed isotropic temperature factors in idealized positions and refined as riding atoms. Molecular diagrams were generated using ORTEP 3.[25] Selected bond distances and angles are presented in Tables 4 and 5. Further details relating to each structure determination are given below.

Tp^{iPr}MoOS(OC$_6$H$_4{}^s$Bu-2) (1). Crystals were obtained as small red-brown plates by diffusion of hexane into dichloromethane solutions at −30 °C. To augment weak high angle reflections, the data set was recollected employing 90 s frames. Refinements were carried out on reflections with $2\theta < 45°$ due to the absence of high angle reflections.

Tp^{iPr}MoOS(OC$_6$H$_4{}^t$Bu-2) (2). Crystals were obtained as dark red blocks by cooling a saturated solution in acetonitrile to −4 °C. Analysis indicated four distinct electron density peaks associated with disorder of the oxo and sulfido ligands over two sites. Assignment of oxo and sulfido ligands, O(2)/O(2A) and S(1)/S(1A), respectively, were made according to peak size and distance from the molybdenum atom. Partial site occupancies were assigned to each atom and refined with bond distance constraints of 1.68 Å for Mo−O(2)/Mo−O(2A) and 2.15 Å for Mo−S(1)/Mo−S(1A) (standard deviations restrained to 0.005 Å). Improved statistical measures of agreement were obtained by applying least-squares refinements on data from $2\theta = 45°$. However, this reduction of reflection data resulted in an unacceptable data/parameter ratio, and as a consequence all reflections out to $2\theta = 50°$ were included in the refinement. The application of the checking program PLATON[26] did not detect any symmetry discrepancies or solvent molecules.

Tp^{iPr}MoOS(OC$_6$H$_4$Ph-4) (3) (1.5MeCN solvate). Crystals were grown by cooling a saturated solution of the complex in acetonitrile. The oxo (O(2)/O(2′)) and sulfido (S(1)/S(1′)) ligands were disordered over two sites, with the major occupancy of 0.61. The Mo−S(1) and Mo−S(1′) distances were restrained to 2.15 Å, and the Mo−O(2) and Mo−O(2′) distances to 1.68 Å. The actual distances were refined to Mo−S(1)/S(1′) 2.206 Å and Mo−O(2)/O(2′) 1.656 Å.

(23) Sheldrick, G. M. *SHELXS-97 Program for Crystal Structure Solution*; University of Göttingen: Germany, 1993.
(24) Sheldrick, G. M. *SHELXL-97 Program for Crystal Structure Refinement*; University of Göttingen: Germany, 1997.
(25) Farrugia, L. J. *J. Appl. Crystallogr.* **1997**, *30*, 565.
(26) (a) Spek, A. L. *PLATON, A Multipurpose Crystallographic Tool*; Utrecht University: Utrecht, The Netherlands, 1998. (b) Spek, A. L. *Acta Crystallogr., Sect. A* **1990**, *46*, C34.

Table 3. Crystallographic Data

	1	**2**	**3**·1.5MeCN	**5**	**8**	**11**
formula	$C_{28}H_{41}BMoN_6O_2S$	$C_{28}H_{41}BMoN_6O_2S$	$C_{33}H_{41.5}BMoN_{7.5}O_2S$	$C_{32}H_{49}BMoN_6O_2S$	$C_{36}H_{56}Mo_2N_{12}B_2O_3S_2$	$C_{28}H_{34}BMoN_6O_2S$
fw	632.49	632.49	714.05	688.15	982.1	625.42
crystal syst	triclinic	triclinic	monoclinic	triclinic	monoclinic	orthorhombic
space group	$P\bar{1}$	$P\bar{1}$	$C2/c$	$P\bar{1}$	$P2_1/c$	$Pbca$
a, Å	8.628(2)	8.572(1)	23.424(3)	11.544(3)	17.9488(9)	16.101(5)
b, Å	12.607(3)	13.009(1)	8.5370(10)	11.580(3)	19.1027(10)	17.766(5)
c, Å	15.573(4)	14.568(1)	35.313(4)	17.527(4)	31.9945(17)	20.420(5)
α, deg	76.061(4)	81.325(3)	90	80.907(5)	90	90
β, deg	77.347(3)	85.151(2)	93.073(2)	70.853(5)	102.194(1)	90
γ, deg	75.608(3)	80.160(3)	90	80.146(4)	90	90
V, Å^3	1569.4(6)	1579.5(3)	7051.6(14)	2167.5(9)	10723.1(1)	5841(3)
Z	2	2	8	2	4	8
ρ_{calcd} (g/cm^3)	1.336	1.330	1.345	1.165	1.217	1.422
μ (cm^{-1})	5.18	5.15	4.71	3.87	5.86	5.57
R_1[a]	0.0583	0.0706	0.0758	0.0583	0.0633	0.0512
wR_2[b]	0.1249	0.1216	0.1630	0.1485	0.1889	0.1022

[a] $R_1 = \sum||F_o| - |F_c||/\sum |F_o|$. [b] $wR_2 = \{[\sum w(F_o^2 - F_c^2)^2/\sum(w|F_o^2|)^2]\}^{1/2}$.

Table 4. Selected Bond Distances (Å) and Angles (deg)

distance/angle	**1**	**2**[a]	**3**·1.5MeCN[a]	**5**	**11**
Mo−O(2)	1.692(5)	1.677(5)	1.656(12)	1.681(3)	2.004(4)
Mo−S(1)	2.132(2)	2.193(3)	2.164(4)	2.348(1)	2.388(2)
Mo−O(1)	1.885(4)	1.903(4)	1.926(4)	1.937(3)	1.696(4)
Mo−N(11)	2.312(5)	2.338(5)	2.333(5)	2.379(4)	2.363(5)
Mo−N(21)	2.305(5)	2.346(4)	2.300(5)	2.218(3)	2.195(6)
Mo−N(31)	2.193(6)	2.199(4)	2.225(5)	2.188(3)	2.211(6)
O(1)−C	1.351(8)	1.362(6)	1.351(7)	1.365(5)	1.302(8)
S(1)−S(1′	−	−	−	2.091(2)	−
O(2)−Mo−S(1)	103.68(16)	101.7(5)	103.6(5)	99.80(10)	81.18(13)
O(2)−Mo−O(1)	102.4(2)	99.2(6)	104.0(5)	103.89(14)	102.7(2)
O(2)−Mo−N(11)	162.7(2)	170.0(4)	165.1(5)	170.14(13)	87.85(18)
O(2)−Mo−N(21)	85.2(2)	91.7(5)	88.9(5)	92.64(13)	166.86(19)
O(2)−Mo−N(31)	88.9(2)	93.3(5)	89.3(5)	91.92(15)	92.70(19)
S(1)−Mo−O(1)	100.78(15)	99.89(16)	100.47(19)	95.38(5)	101.21(17)
S(1)−Mo−N(11)	90.46(14)	86.34(14)	88.72(17)	85.39(9)	91.71(14)
S(1)−Mo−N(21)	166.38(15)	164.37(14)	166.20(18)	164.64(10)	94.19(16)
S(1)−Mo−N(31)	91.95(15)	91.83(16)	94.10(19)	88.00(10)	168.54(15)
O(1)−Mo−N(11)	84.31(19)	85.04(15)	81.52(17)	83.82(12)	164.3(2)
O(1)−Mo−N(21)	87.07(18)	85.74(15)	81.94(17)	90.31(12)	90.2(2)
O(1)−Mo−N(31)	160.34(19)	160.68(15)	157.20(17)	162.97(13)	89.5(2)
N(11)−Mo−N(21)	79.17(19)	79.60(16)	78.15(18)	81.04(13)	80.0(2)
N(11)−Mo−N(31)	80.6(2)	80.41(15)	81.38(18)	79.81(14)	78.3(2)
N(21)−Mo−N(31)	77.77(19)	79.22(16)	79.89(18)	82.56(13)	89.6(2)
Mo−S(1)−S(1′	−	−	−	105.96(8)	−
Mo−O−C	148.9(4)	152.1(3)	135.5(4)	139.6(3)	122.8(4)
Mo−S(1)−C(39)	−	−	−	−	96.6(2)

[a] Values for one of two (disordered) oxo and sulfido positions cited.

Table 5. Selected Distances and Angles for **8** (for molecule 1)

distance (Å)	at Mo(1)	at Mo(2)	distance (Å)	at Mo(1)	at Mo(2)
Mo═O	1.673(5)	1.673(5)	Mo−N(21)/N(51)	2.248(7)	2.254(7)
Mo−S	2.333(2)	2.346(2)	Mo−N(31)/N(61)	2.243(6)	2.227(6)
Mo−O	1.861(5)	1.858(5)	S(1)−S(2)	2.146(3)	−
Mo−N(11)/N(41)	2.380(6)	2.392(7)	Mo(1)···Mo(2)	3.641(1)	−

angle (deg)	at Mo(1)	at Mo(2)	angle (deg)	at Mo(1)	at Mo(2)
O═Mo−S	99.22(19)	99.6(2)	S−Mo−N(31)/N(61)	97.17(18)	97.63(18)
O═Mo−O	107.0(2)	107.0(2)	O−Mo−N(11)/N(41)	89.4(2)	88.2(2)
O═Mo−N(11)/N(41)	159.8(2)	160.8(2)	O−Mo−N(21)/N(51)	91.8(2)	91.5(2)
O═Mo−N(21)/N(51)	86.9(2)	86.4(3)	O−Mo−N(31)/N(61)	163.8(2)	163.8(2)
O═Mo−N(31)/N(61)	89.1(2)	89.0(2)	N−Mo−N	74.4(2)−86.8(2)	75.6(2)−86.6(2)
S−Mo−O	82.68(16)	82.78(15)	Mo−S−S	108.47(10)	107.66(10)
S−Mo−N(11)/N(41)	94.33(17)	93.91(16)	Mo(1)−O(3)−Mo(2)	156.5(3)	−
S−Mo−N(21)/N(51)	172.72(18)	172.7(2)			

[Tp^{iPr}MoO(OC$_6$H$_3$^{t}Bu$_2$-3,5)]$_2$(μ-S$_2$) (5). Crystals were grown from a cooled hexane solution at −30 °C. The application of the PLATON (SQUEEZE)[27] program indicated the presence of a solvent cavity occupied by an electron density equivalent to that of a hexane molecule. Attempts to model the disordered solvent using standard techniques were unsuccessful. Consequently, eleven peaks of unassigned electron density in the electron difference map were assigned as carbon atoms with common isotropic displacement parameters. The site occupation

factors were allowed to refine resulting in a combined total of 6.24 carbon atoms, consistent with a hexane solvent molecule. Solvent hydrogen atoms were not included in the model.

[Tp^{iPr}MoO]$_2$(μ-S$_2$)(μ-O) (8). Dark purple-brown crystals were grown by slow evaporation of a dichloromethane solution of the complex. The asymmetric unit was found to possess two independent molecules; attempts to locate a cell with higher symmetry than $P2_1/c$ using the checking program PLATON[26] were unsuccessful.

Tp^{iPr}MoO(OSC$_{10}$H$_6$) (11). Crystals were grown by slow diffusion of hexane into a dichloromethane solution of the complex. Data were collected on an Enraf-Nonius Kappa CCD diffractometer equipped with graphite monochromated Mo Kα radiation over the range $4° < 2\theta \leq 45°$.

X-ray Absorption Spectroscopy. Sulfur K-edge X-ray absorption studies were performed at the Stanford Synchrotron Radiation Laboratory (SSRL) with the SPEAR storage ring containing 75−100 mA at 3.0 GeV. Experiments were performed on Beamline 6-2 using an Si(111) double crystal monochromator and a wiggler field of 0.85 T. Harmonic rejection was accomplished using a flat nickel coated mirror downstream of the monochromator effecting a cutoff energy of 4500 eV. Incident X-ray intensity was monitored using an ion chamber contained in a (flowing) helium-filled flight path. Energy resolution was optimized by decreasing the vertical aperture upstream of the monochromator and quantitatively determined to be 0.51 eV by measuring the width of the 2471.4 eV 1s → π* 3(b$_1$) transition of gaseous SO_2, which corresponds to a transition to a single orbital, rather than to a band of orbitals (in contrast to solid standards).[28] X-ray absorption was monitored by recording total electron yield, and the energy scale was calibrated with reference to the lowest energy peak of the sodium thiosulfate standard ($Na_2S_2O_3 \cdot 5H_2O$) which was assumed to be 2469.2 eV.[29] Data were analyzed using the EXAFSPAK suite of computer programs (http://ssrl.slac.stanford.edu/EXAFSPAK.html), and no smoothing or related operations were performed on the data. Pre-edge features were estimated by curve-fitting to a sum of pseudo-Voigt peaks using the program EDG_FIT (pseudo-Voigt deconvolution).[30]

Results and Discussion

The Tp^{iPr}MoO(OAr)(OPEt$_3$)/[S] System. Atom transfer reactions were employed to convert the dioxo-Mo(VI) complexes, Tp^{iPr}MoO$_2$(OAr), into oxosulfido-Mo(VI) species, via isolable oxo(phosphine oxide)-Mo(IV) intermediates (Scheme 1).[19,20] Direct sulfidation of the dioxo complexes, a method employed in the preparation of other oxosulfido-Mo(VI) species,[11,12] did not yield tractable products. Sulfur atom transfer from propylene sulfide to Tp^{iPr}MoO(OAr)(OPEt$_3$) resulted in a variety of products depending on the nature of the OAr ligand, the reaction conditions, and the workup procedures. In every case, the initial step appears to be replacement of the phosphine oxide ligand by a terminal sulfido ligand, with concomitant oxidation of Mo(IV) to Mo(VI) and the formation of monomeric oxosulfido species.

Dark red, monomeric **1**−**3** were isolated only under *anhydrous, anaerobic* conditions. Complex **1** precipitated as the initial product in reactions with high reagent concentrations and short (30 min) reaction times; prolonged reactions (ca. 1 day) resulted in the conversion of **1** to **9**. Related transformations were not observed for **2** or **3** (vide infra). Monomeric **1**−**3** are highly soluble in chlorinated solvents and, to a lesser extent, in MeCN, DMF, diethyl ether, alcohols, toluene, and hexane. Workups under *aerobic* conditions employing *wet* solvents resulted in isolation of the air-stable, μ-oxo complex, **8**, that is soluble in chlorinated solvents, alcohols, DMF, benzene, and toluene and slightly soluble in hexanes.

Dark maroon-red, dimeric **4**−**7** were also isolated under *anhydrous, anaerobic* reaction and workup conditions; *aerobic* workup with *wet* solvents again produced **8**. Reactions of the 2-phenylphenolate and 1-naphtholate derivatives were complicated and produced inseparable mixtures of oxosulfido and molybdenyl complexes under anaerobic conditions (vide infra); aerobic workup allowed the isolation of mixtures of **8** and molybdenyl complexes from these reactions. Only molybdenyl complexes were isolated from the reactions of Tp^{iPr}MoO(OC$_{10}$H$_7$-2)(OPEt$_3$) or Tp^{iPr}MoO(OC$_6$H$_4$^{t}Bu-4)(OPEt$_3$) with propylene sulfide, after either *anaerobic* and *aerobic* workup (vide infra). Dimeric **4**−**7** are soluble in chlorinated solvents, MeCN, DMF, diethyl ether, and alcohols and slightly soluble in hexanes (**7** being the least soluble); all complexes were *monomeric* in solution (vide infra).

Hydrolysis of Tp^{iPr}MoOS(OAr), through aerobic workup of reactions (vide supra) or addition of water to solutions of Tp^{iPr}MoOS(OAr), resulted in the formation of purple-brown, diamagnetic **8**. In principle, **8** may arise from hydrolysis of (prevalent) monomeric species or (undetectable) dimeric solution species; its formation from strictly monomeric **1**−**3** suggests that the hydrolysis of monomers is responsible for its formation. A possible reaction sequence involves ligand exchange to yield Tp^{iPr}MoOS(OH), followed by condensation producing dinuclear **8**. We are currently pursuing the isolation and study of the putative Tp^{iPr}MoOS(OH) complex as a functional model for the Mo hydroxylases.

Certain oxosulfido complexes are unstable with respect to molybdenyl complexes. Prolonged (>12 h) reaction of Tp^{iPr}MoO(OC$_6$H$_4$^{s}Bu-2)(OPEt$_3$) with propylene sulfide (under anhydrous, anaerobic conditions) led to the isolation of the molybdenyl complex **9** rather than the initial product of the reaction, **1**. Isolated **1**, when returned to solution (in MeCN or toluene) or allowed to stand for long periods in the solid state, also converted into **9** (again, this was not the case for **2** and **3** (vide infra)). Molybdenyl complexes formed quickly (<1 h) in the reactions of Tp^{iPr}MoO(OAr)(OPEt$_3$) (OAr = OC$_6$H$_4$Ph-2, OC$_6$H$_4$^{t}Bu-4, 1-OC$_{10}$H$_7$, 2-OC$_{10}$H$_7$) with propylene sulfide and hampered the isolation of pure oxosulfido or μ-disulfido complexes. Complexes **2**−**6** are stable with respect to molybdenyl complexes. The brown, air-stable molybdenyl complexes are readily soluble in chlorinated solvents, diethyl ether, THF, and acetonitrile but slightly less so in alcohols and hexane.

At this time, it is premature to speculate about the mechanism of formation of the molybdenyl complexes; however, the following observations may be relevant. To date, we have been unable to identify an Mo-containing byproduct or establish the fate of the hydrogen atom removed in the reactions (eq 1). In

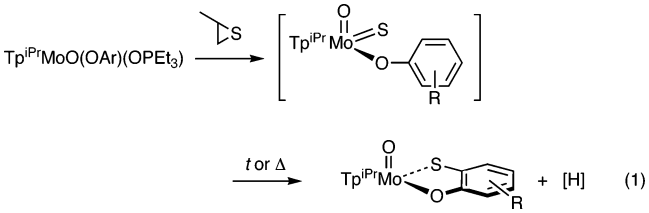

(1)

(27) van der Sluis, P.; Spek, A. L. *Acta Crystallogr., Sect. A* **1990**, *46*, 194−201.
(28) Song, I.; Rickett, B.; Janavicius, P.; Payer, J. H.; Antonio, M. R. *Nucl. Instrum. Methods Phys. Res., Sect. A* **1995**, *360*, 634−641.
(29) Sekiyama, H.; Kosugi, N.; Kuroda, H.; Ohta, T. *Bull. Chem. Soc. Jpn.* **1986**, *59*, 575−579.
(30) Pickering, I.; George, G. N. *Inorg. Chem.* **1995**, *34*, 3142−3152.

situ S K-edge XAS studies revealed initial growth of pre-edge features due to oxosulfido species and their subsequent disappearance upon molybdenyl complex formation. As well, pure **1** has been observed to undergo a thermally assisted conversion to **9** in solution and the solid state. Therefore, it appears that oxosulfido-Mo(VI) complexes are the immediate precursors of the molybdenyl complexes, the sulfido ligand attacking a coligand C−H group with resulting C−S bond formation (eq 1). We are unaware of any precedent for aromatic C−H bond activation by terminal sulfido ligands, although, to some extent (viz., without leading to C−S bond formation), it is implicit in mechanisms presented for Mo hydroxylases.[1−5] Related molybdenyl complexes have been prepared by reacting Tp^*MoOCl_2 with 2-mercaptophenols, but these metathetical syntheses are unrelated to the reactions described here.[31] A mechanistic description of this novel reaction will be the goal of future studies.

The oxosulfido complexes undergo sulfur atom transfer (SAT) rather than oxygen atom transfer when reacted with tertiary phosphines (the product of the reaction depends on the solvent employed). This is consistent with the presence of an Mo═S π^* LUMO, rendering the sulfido more electrophilic than the oxo ligand. SAT has also been observed in the reactions of phosphines with $MoOS(OSiPh_3)_2L$[13] and $Tp^*MoOS(S_2PR_2)$.[14] Given the use of SAT to prepare the $Tp^{iPr}MoOS(OAr)$ complexes, it is not surprising that they are effective catalysts for SAT from propylene or cyclohexene sulfides to tertiary phosphines. Further studies of the SAT chemistry of the title complexes will be reported at a later date.

Characterization of $[Tp^{iPr}MoOS(OAr)]_n$ Complexes. Microanalytical (Supporting Information) and mass spectrometric (Table 1) data were consistent with the proposed formulations. The mass spectra of all the complexes exhibited an $[M + H]^+$ peak cluster indicative of the presence of monomeric complexes in solution. The observation of weak peak clusters due to dimeric species (for **4**−**7** only) is attributed to dimerization during electrospray ionization. Osmometric molecular mass determinations confirmed the monomeric nature of **4** (610 ± 30, calcd 632), **5** (708 ± 35, calcd 689), **6** (660 ± 35, calcd 655) and **7** (594 ± 30, calcd 576) in solution.

The solid-state IR spectra of monomeric **1**−**3** exhibited strong bands at ca. 910 and 485 cm^{-1}, assigned to ν(Mo═O) and ν(Mo═S) vibrations, respectively (Table 1). The energies of the ν(Mo═O) bands were significantly lower than those of the oxo(phosphine oxide)-Mo(IV) precursors (ca. 950 cm^{-1})[20] and the dimeric species (vide infra). They are, however, within the documented range for ν(Mo═O) vibrations.[12] Bands in the 520−460 cm^{-1} region are characteristic of terminal sulfido ligands.[12] The low value of ν(Mo═S) is suggestive of a metal−sulfur double bond[22] rather than a formal triple bond as observed for Tp^*MoSCl_2 (ν(Mo≡S) 523 cm^{-1}).[32] The ν(W═O) and ν(W═S) bands of related Tp*WOS(OAr) complexes are observed at ca. 935 and 480 cm^{-1}, respectively.[33] The ν(Mo═O) and ν(Mo═S) bands in the oxosulfido complexes above are in good agreement with the corresponding values for xanthine oxidase (899 and 474 cm^{-1}, respectively) determined by resonance Raman spectroscopy.[34]

The solid-state IR spectra of dimeric **4**−**7** exhibited a single ν(Mo═O) band at 924−940 cm^{-1} but no significant band in the ν(Mo═S) region. However, consistent with the presence of monomers in solution, strong ν(Mo═O) and ν(Mo═S) bands at 913 and 484 cm^{-1}, respectively, were evident in solution (CH_2Cl_2) IR spectra. The presence of the Tp^{iPr} ligand in all complexes was confirmed by the observation of ligand bands (e.g., ν(BH) ca. 2550 cm^{-1}, ν(CN) ca. 1510 cm^{-1}). Bands characteristic of the phenolate ligands were observed at ca. 1630−1570 cm^{-1} (ν(C−O)) and ca. 1260 cm^{-1} ($\nu(CC)_{ring}$). On occasions, small IR bands in the regions expected for monomers (vide supra) were observed in samples of the dimers. There is also S K-edge XAS evidence for a population of monomers in samples of the dimers (vide infra).[35]

The expected C_1 symmetry of the chiral $Tp^{iPr}MoOS(OAr)$ complexes was confirmed by NMR spectroscopy, which revealed the inequivalence of all protonic groups (Table 1). The phenolate 6-H protons of **1** and **2** were shielded by ca. 2.1 ppm compared to the free ligand, an observation consistent with the maintenance of the solid-state structures (with the 6-H proton in the Tp^{iPr} ring shielding zone (vide infra)) in solution. Two of the isopropyl methyl group resonances are also noticeably shielded, by ca. 0.4 ppm, in **1** and **2**. The NMR spectra of the dioxo-Mo(VI) analogues show similar features.[19,20] The remaining complexes have varying degrees of conformational flexibility, permitting the benzene ring to reside outside of the pyrazole shielding zone; consequently, their ring proton resonances are unperturbed. The complicated ^1H NMR spectrum of **1** (Supporting Information) is attributed to the presence of stereoisomers, resulting from the chirality at Mo *and* the C-2 atom of the *sec*-butyl group. Chirality at Mo can be defined as *R* or *S* when Tp^{iPr} is treated as a single ligand in a pseudo-tetrahedral complex. In principle, **1** can form four stereoisomers, enantiomeric (*R*,*R*)/(*S*,*S*) and meso (*R*,*S*)/(*S*,*R*) pairs.

The optical spectra of the complexes displayed two moderately intense absorption bands at ca. 510 and 410 (shoulder) nm (Table 1). These features are completely absent from the spectra of related dioxo complexes and are assigned to S → Mo LMCT transitions. Detailed analysis of the optical and magnetic circular dichroism spectra of **6** and **7**[17] has allowed the 510 nm band to be assigned to nearly degenerate electronic $\psi(S^v(p_z))$ → $\psi(Mo(d_{xz,yz}))$ transitions (where the υ(ertical) direction is aligned with *z* (Mo═O)) and the 410 nm shoulder to be assigned to a phenolate-based $\psi(O^v(p_z))$ → $\psi(Mo(d_{xy}))$ MLCT.[22] Multiple transitions are responsible for the very strong absorption band at higher energy.[22]

Cyclic voltammetric data for the oxosulfido complexes and their dioxo analogues are summarized in Table 6. A single, reversible, one-electron reduction was observed for each complex, the resulting anion being stable on the cyclic voltammetric time scale. Consistent with trends observed in related systems,[33,36] the oxosulfido complexes exhibited reduction potentials ca. 300 mV more positive than their dioxo ana-

(31) Cleland, W. E., Jr.; Barnhart, K. M.; Yamanouchi, K.; Collison, D.; Mabbs, F. E.; Ortega, R. B.; Enemark, J. H. *Inorg. Chem.* **1987**, *26*, 1017−1025.
(32) Young, C. G.; Enemark, J. H.; Collison, D.; Mabbs, F. E. *Inorg. Chem.* **1987**, *26*, 2925−2927.
(33) Eagle, A. A.; Tiekink, E. R. T.; George, G. N.; Young, C. G. *Inorg. Chem.* **2001**, *40*, 4563−4573.
(34) Maiti, N. C.; Tomita, T.; Kitagawa, T.; Okamoto, K.; Nishino, T. *J. Biol. Inorg. Chem.* **2003**, *8*, 327−333.
(35) We are endeavoring to find conditions that result in the crystallization of monomeric forms of the dimeric species. Modification of the synthesis of **7** to parallel those reported for **4** and **5** appears to produce a solid highly enriched in monomer (as shown by IR and S K-edge XAS studies). Further investigations of the monomer−dimer equilibria are underway.

Table 6. Electrochemical Data for $Tp^{iPr}MoOS(OAr)$ (by Ascending $E_{1/2}$)[a]

compd (Ar, no.)	$E_{1/2}$ (V)	E_{pc} (V)	E_{pa} (V)	I_{pa}/I_{pc}	ΔE_{pp} (mV)	$E_{1/2}$[b] (V)	ΔE[c] (mV)
$C_6H_4{}^tBu$-2 (**2**)	−0.626	−0.587	−0.665	0.96	78	−1.045[d]	−
$C_6H_4{}^sBu$-2 (**1**)	−0.552	−0.515	−0.589	0.95	74	−0.844	292
$C_6H_3{}^tBu_2$-3,5 (**5**)	−0.533	−0.503	−0.563	1.01	60	−0.855	322
$C_6H_4{}^tBu$-3 (**4**)	−0.502	−0.471	−0.533	0.95	62	−0.814	312
Ph (**7**)	−0.479	−0.448	−0.510	0.98	62	−0.780	301
C_6H_4Ph-4 (**3**)	−0.460	−0.421	−0.499	0.99	78	−0.751	291

[a] For $Tp^{iPr}MoOS(OAr)$, data at 20 mV s^{-1} in MeCN vs SCE. [b] $E_{1/2}$ data for $Tp^{iPr}MoO_2(OAr)$ analogue in MeCN (from refs 18 and 19). [c] Difference in $E_{1/2}$ values: $E_{1/2}$(oxosulfido) − $E_{1/2}$(dioxo). [d] Measured in dichloromethane (direct comparison prohibited).

logues.[18,19] The origin of this positive shift in reduction potential can be rationalized by differences in the electronic manifolds of $[MO_2]^{2+}$ vs $[MOS]^{2+}$ (M = Mo,[22] W[33]) complexes. The π^* LUMO of the dioxo complexes is high in energy, and a large negative potential is required for reduction (i.e., LUMO to SOMO conversion). The HOMO and LUMO of the oxosulfido complexes are Mo/S-based due to the highly stabilized oxo 2p orbitals. The LUMO is Mo═S antibonding in nature and consists of a symmetry adapted linear combination of Mo $4d_{xy}$ and S $3p_x$ atomic orbitals. The M═S based LUMO of $[MOS]^{2+}$ is relatively low in energy compared to the LUMO of $[MO_2]^{2+}$, resulting in a positive shift in reduction potential.

The redox potentials of these and related dioxo-Mo(VI) complexes[18,19] also depend on the nature of the coligand. Thus, substitution of the coligand can induce shifts in reduction potential over a 200 mV range (Table 6). However, there is no clear correlation between reduction potential and reactivity. For example, **4** and **5**, with reduction potentials around −0.515 V, are involved in monomer−dimer equilibria. However, **1**−**3**, with reduction potentials of −0.552, −0.626, and −0.460 V, respectively, are strictly monomeric despite the reduction of the latter being electrochemically facile. Thus, these data do not form a clear pattern that would support an electrochemical rationale for the dimerization (or otherwise) of the complexes.

Sulfur Ligand X-ray Absorption Spectroscopy. Ligand K-edge X-ray absorption spectroscopy (XAS) provides structural and electronic information at a number of levels. At a qualitative level, the presence of intense pre-edge transitions confirms the existence of particular ligands, geometries, or electronic configurations. Thus, the presence of terminal sulfido ligands in metal−sulfur species is indicated by the observation of strong sulfur K pre-edge features associated with S(1s) → π^*(S 3p + M *n*d) transitions.[17,33] At a quantitative level, ligand K-edge XAS may be employed to evaluate the contribution of ligand orbitals to the frontier molecular orbitals, i.e., the degree of metal−ligand covalency, in metal complexes.[37] The intensities of the S K pre-edge transitions of terminal sulfido complexes provide a quantitative assessment of Mo═S covalency. This is evident in a detailed study of **7** by S K-edge XAS and complementary spectroscopic and computational techniques.[22] This study revealed a high degree of covalency in the Mo═S based frontier orbitals and permitted an assessment of the orbital character and energy of these orbitals, the results and conclusions of which are mirrored in the following observations relating to **1**−**3**.

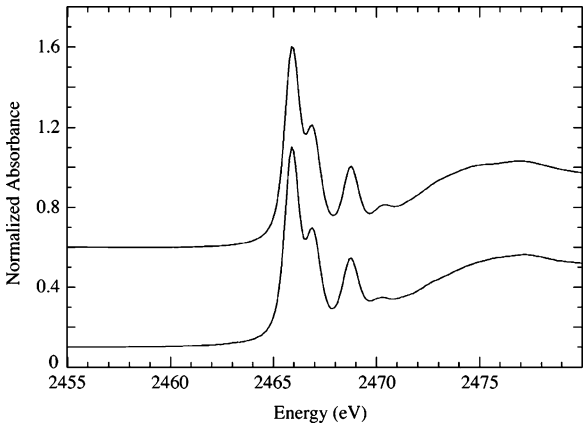

Figure 1. Sulfur K-edge X-ray absorption spectra of **1** in solution (top) and solid (bottom) states.

The solution and solid-state X-ray absorption spectra of **1** are shown in Figure 1. The spectra clearly indicate the existence of monomeric species, with unperturbed oxosulfido-Mo(VI) units, *in both phases*. Analogous pre-edge features are observed in the solid and solution spectra of **2** and **3**. The presence of monomers in the solid state has been confirmed by X-ray diffraction of all three complexes (vide infra). The pre-edge region of the solid-state spectrum of **1** was fitted with three pseudo-Voigt functions at 2465.9, 2466.9, and 2468.8 eV, with an integrated intensity ratio of 1:0.51:0.35, respectively. These calculations suggest that the most significant S character is observed in the lowest energy (S 3p + Mo 4d) orbital which, according to the C_1 symmetry of **1** (z direction collinear with Mo═O), involves the Mo d_{xy} orbital. This is consistent with EPR studies of a ^{33}S labeled Very Rapid xanthine oxidase intermediate that demonstrate that the SOMO possesses approximately 38% S 3p character.[38,39] DFT calculations performed on a computational model based on the crystal structure parameters of **1** determined that the lowest energy Mo-based acceptor orbitals d_{xy}, $d_{xz,yz}$, and $d_{x^2-y^2}$ possess significant sulfur character. These results are comparable with the S K-edge XAS integrated ratio of 1.00:0.50:0.49 reported for **7** and indicate the presence of analogous electronic structures.[22]

The solid and solution S K-edge X-ray absorption spectra of **5**, displayed in Figure 2, are analogous to those reported for **7**.[17] Similar spectra were also recorded for complexes **4** and **6**. All solid-state spectra feature a broad, multicomponent absorption with a maximum around 2469.5 eV. The component bands are likely to arise from S(1s) → σ^*(S−S) and S(1s) → σ^*(Mo−S) transitions associated with the bridging disulfido ligand. Crystallographic characterization of **5** (vide infra) and **7**[17] has confirmed the presence of dimeric species in the solid state. A very small shoulder at ca. 2464 eV is evidence for a small population of monomers in the solid samples examined.[35] In contrast, the solution spectra of the complexes exhibit distinct pre-edge features characteristic of terminal sulfido species. The solution spectrum of **5** (Figure 2) possesses three distinct pre-edge features, at 2465.9, 2467.1, and 2469.1 eV. Solution spectra are solvent independent to the limit of analysis. These observa-

(36) Bristow, S.; Garner, C. D.; Pickett, C. J. *J. Chem. Soc., Dalton Trans.* **1984**, 1617−1619.
(37) Solomon, E. I.; Hedman, B.; Hodgson, K. O.; Dey, A.; Szilagyi, R. K. *Coord. Chem. Rev.* **2005**, *249*, 97−129.
(38) Wilson, G. L.; Greenwood, R. J.; Pilbrow, J. R.; Spence, J. T.; Wedd, A. G. *J. Am. Chem. Soc.* **1991**, *113*, 6803−6812 and references therein.
(39) George, G. N.; Bray, R. C. *Biochemistry* **1988**, *27*, 3603−3609.

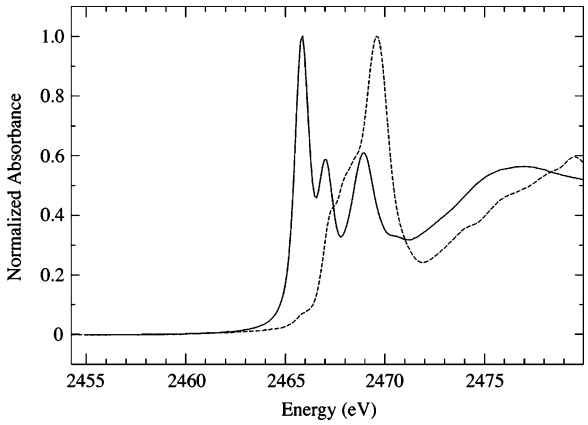

Figure 2. Sulfur K-edge X-ray absorption spectra of **5** in MeCN solution (—) and the solid state (- - -).

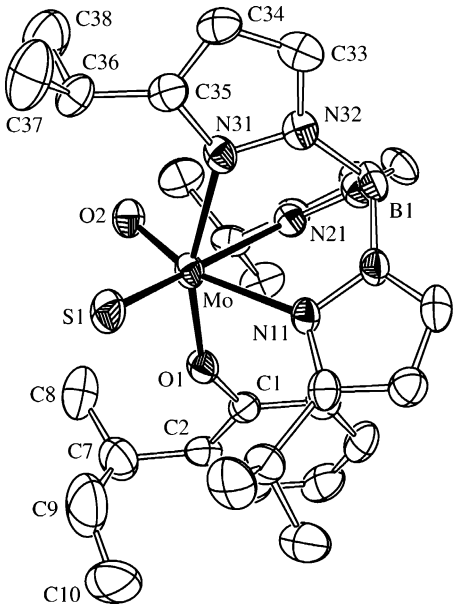

Figure 3. ORTEP projection of **1** at the 30% probability level. Hydrogen atoms have been omitted for clarity.

tions support a monomer/dimer interconversion, the monomer existing in solution, the dimer predominating in the solid.

Solid State Structures of 1−3. The crystal structures of **1**−**3** were determined by X-ray diffraction. Only *rac*-**1** (Figure 3) exhibited ordering of the oxo and sulfido ligands; thus, although the structure description that follows pertains to all three structures, only metrical data for **1** are quoted.

Monomeric **1**−**3** exhibit distorted octahedral geometries, the Mo atom being coordinated by a facial, tridentate Tp$^{i\mathrm{Pr}}$ ligand and mutually cis monodentate oxo, sulfido, and phenolate ligands. The absence of close contacts between S(1) and neighboring groups confirms the presence of an unperturbed terminal sulfido ligand. Distortions from octahedral geometry include acute N−Mo−N angles (av. 79.2°), an O(2)−Mo−S(1) angle of 103.68(16)°, and an O(1)−Mo−N(31) angle of 160.34(19)°. The atoms in the equatorial girdle, viz., O(2), S(1), N(11), and N(21), are essentially planar with an rms deviation of only 0.0177 Å. The central molybdenum atom is positioned 0.165(2) Å below this plane, toward O(1). These distortions are commonly observed for *cis*-bis(chalcogenido) tris(pyrazolyl)borate complexes.[12]

The Mo−O(2) distance of 1.692(5) Å is typical of a terminal oxo group but shorter than the Mo═O distance of 1.732(12) Å reported for MoOS(ONC$_5$H$_{10}$)$_2$[40] and the range determined by EXAFS for MoOS(OSiPh$_3$)$_2$L complexes (1.71−1.72 Å).[13] The short Mo−S(1) distance of 2.132(2) Å is comparable to values reported for MoOS(ONC$_5$H$_{10}$)$_2$ (2.106(5) Å), for MoOS(OSiPh$_3$)$_2$L (2.18−2.19 Å by EXAFS), and in the Mo hydroxylases (ca. 2.15 Å by EXAFS[1−5]). The obtuse O(2)−Mo−S(1) angle of 103.68(16)° is typical of six-coordinate, *cis*-dichalcogenido species.[12] The structural parameters for **1** are also concordant with values for related oxosulfido-W(VI) complexes, including Tp*WOS(S$_2$PPh$_2$)[41] and (*R*,*S*)-Tp*WOS{(−)-mentholate}.[33]

The Mo−O(1) distance of 1.885(4) Å is slightly shorter than those typical of other Mo−OAr complexes.[42] The phenoxide ligand lies out of the pseudo-mirror plane (in this case the O(1), Mo, N(31) plane, with an rms deviation of 0.0063 Å) toward the pyrazole group containing N(21). Due to steric demands, the *sec*-butyl group projects away from the Tp$^{i\mathrm{Pr}}$ ligand and into the region of the terminal chalcogenide ligands, the sterically less demanding 6-H proton being nestled between the pyrazole rings containing N(11) and N(21). The steric protection afforded by the phenolate substituent is a primary determinant of the stability and reaction pathways of the Tp$^{i\mathrm{Pr}}$MoOS(OAr) complexes (vide infra). Finally, the trans influences exerted by the terminal oxo and sulfido ligands result in a ca. 0.11 Å increase in the Mo−N(11) and Mo−N(21) bond distances relative to unaffected Mo−N(31).

Superposition of Tp$^{i\mathrm{Pr}}$MoOS(OC$_6$H$_4$^{s}Bu-2) and its dioxo analogue (Figure 4a) shows that the complexes are essentially isostructural, apart from a greater shift of the coligand away from the terminal sulfido ligand. The coligand displacement is accompanied by a contraction of the Mo−O(1)−C(1) angle from 161.5(3)° in the dioxo complex to 148.8(3)° in the oxosulfido analogue. Retreat of the ligand from the terminal sulfido unit may be attributed to a combination of intra- and intermolecular (crystal packing) steric influences. Similar comments, relating to a smaller coligand shift, pertain to complex **2** (see Figure 4b). Complexes **1** and **2** were expected to be monomeric on the basis of structure determinations for their dioxo[19] and oxo(phosphine oxide)[19,20] counterparts. Interestingly, the structure of Tp$^{i\mathrm{Pr}}$MoO$_2$(OC$_6$H$_4$Ph-4) contains a phenolate ligand orientation that provides little frontal (viz. O$_3$-face) steric protection to dimerization; the coligand projects away from the oxo ligands and the nearest Mo═O···HC$_{\mathrm{OAr}}$ contacts are ca. 4.7 Å (Figure 5). However, a quite different phenolate ligand orientation is observed for *monomeric* **3** (Figure 5). Here, the ligand is tilted toward the oxo/sulfido ligands, with close Mo═E···HC$_{\mathrm{OAr}}$ contacts of ca. 3.0 Å. Steric conflict between the phenolate and Tp$^{i\mathrm{Pr}}$ groups on adjacent Mo atoms would arise in an *anti*-[Tp$^{i\mathrm{Pr}}$-MoO(OC$_6$H$_4$Ph-4)]$_2$(μ-S$_2$) dimer based on this monomeric unit. The lattice acetonitrile appears to play a role in the energetics of coligand reorientation and the position of the monomer−dimer equilibria.[35]

Solid State Structure of [Tp$^{i\mathrm{Pr}}$MoO(OC$_6$H$_3$^{t}Bu$_2$-3,5)]$_2$(μ-S$_2$). Complex **5** exhibits a dimeric, centrosymmetric structure

(40) Bristow, S.; Collison, D.; Garner, C. D.; Clegg, W. *J. Chem. Soc., Dalton Trans.* **1983**, 2495−2499.
(41) Thomas, S.; Eagle, A. A.; Sproules, S. A.; Hill, J. P.; White, J. M.; Tiekink, E. R. T.; George, G. N.; Young, C. G. *Inorg. Chem.* **2003**, *42*, 5909−5916.
(42) Orpen, A. G.; Brammer, L.; Allen, F. H.; Kennard, O.; Watson, D. G.; Taylor, R. *J. Chem. Soc., Dalton Trans.* **1989**, S1−S83.

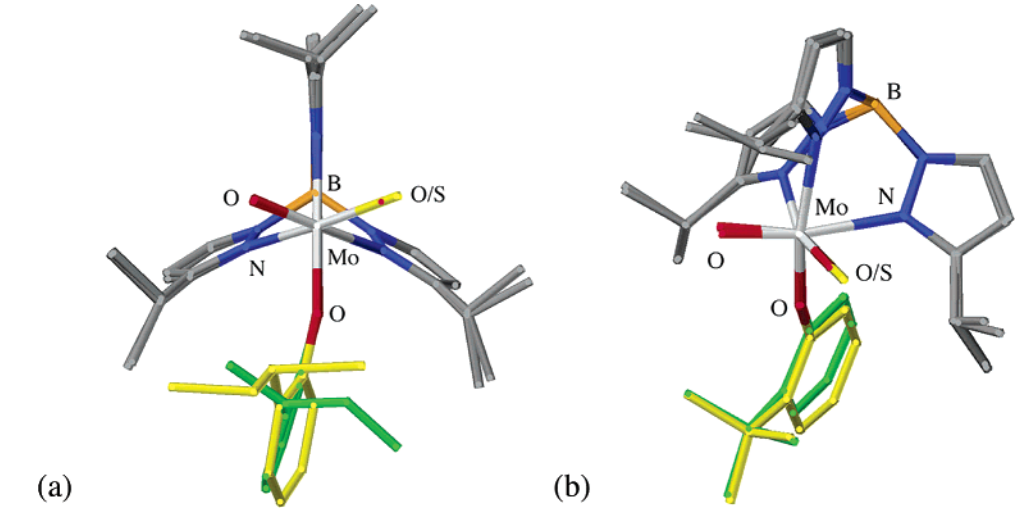

Figure 4. Superposition of the solid-state structures of (a) **1** and $Tp^{iPr}MoO_2(OC_6H_4{}^sBu\text{-}2)$ and (b) **2** and $Tp^{iPr}MoO_2(OC_6H_4{}^tBu\text{-}2)$. The phenolate coligands are colored green and yellow in the oxosulfido and dioxo complexes, respectively.

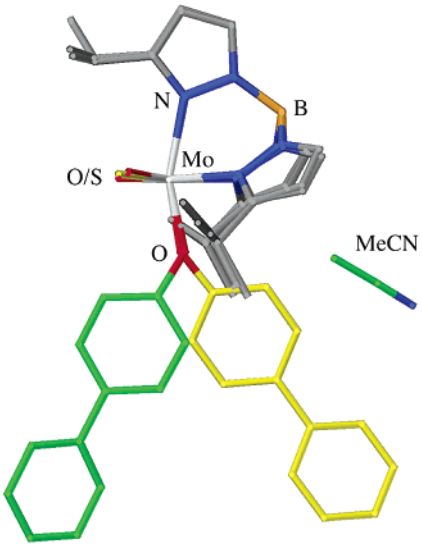

Figure 5. Superposition of the solid-state structures of **3** and $Tp^{iPr}MoO_2(OC_6H_4Ph\text{-}4)$. The phenolate coligands are colored green and yellow in the oxosulfido and dioxo complexes, respectively.

(Figure 6) closely related to the structure of dimeric **7**.[17] Both Mo atoms are coordinated by a facial, tridentate Tp^{iPr} ligand and mutually cis terminal oxo, phenolate, and bridging disulfido ligands, in a distorted octahedral geometry. The terminal oxo ligands adopt an anti disposition across the S—S bridge. Distortions from octahedral geometry include obtuse O—Mo—O/S (av. 99.3°) and acute N—Mo—N (av. 81.1°) angles, leading to trans O/S—Mo—N angles that deviate from 180° (av. 165.9°). These distortions reflect the positioning of the Mo═O(2) unit away from S(1) and O(1) and toward Tp^{iPr}. The O(2)—Mo—S(1) angles, with an average value of 99.4°, are more acute than the corresponding angle in **1** (103.68(16)°). The Mo—O(1)—C(39) angles of ca. 140° reflect the retreat of the coligand toward the Tp^{iPr} moiety during dimerization. This is also observed, but to a lesser extent (144.01(19)°), in **5** and allows the vitiation of the steric protection against dimerization. The more acute Mo—O(1)—C(39) angle contrasts with the corresponding angles in the monomeric complexes (148.9(4)° for **1**) where the bulky substitutents prevent dimerization. The short Mo—O(2) distance of 1.681(3) Å is characteristic of terminal Mo═O bonds, while the long Mo—S(1) and Mo—O(1) bond lengths of 2.3488(12) and 1.937(3) Å, respectively, are typical of single bonds.[42] The trans influence of the oxo ligand results in a lengthening of ca. 0.18 Å for Mo—N(11) relative to the congruent Mo—N(21) and Mo—N(31) distances. The S—S′ distance of 2.091(2) Å is typical of an S—S single bond.[42]

Characterization and Crystal Structure of $[Tp^{iPr}MoO]_2(\mu\text{-}S_2)(\mu\text{-}O)$. Complex **8** was characterized by microanalysis, mass spectrometry, and IR (ν(Mo═O) 942 cm^{-1}), NMR, and UV−vis spectroscopy (Table 1). Like its Tp* analogue, the complex exhibits several very shielded ^{i}Pr NMR resonances and a distinctive UV−visible spectrum (cf. bands at 782, 574, and 425 nm for the Tp* analogue).[43] This complex is generated in a variety of reactions that may, on the basis of the results reported herein, involve the formation of previously unrecognized oxosulfido-Mo(VI) species.[43]

Crystals of **8** contain two independent enantiomeric molecules (see Table 5 for data pertaining to enantiomer **1**). Each molecule is comprised of two distorted octahedral, anti oxo-Mo centers bridged by μ-oxo and μ-disulfido-κS:$\kappa S'$ ligands, and coordinated by facial, tridentate Tp^{iPr} ligands (Figure 7). The typically short Mo═O distances lie in a narrow range of 1.672(5)−1.675(5) Å. The bridging core is characterized by average Mo—(μ-O) and Mo—(μ-S) distances of 1.860 Å and 2.339 Å, respectively, and Mo—O—Mo, (μ-O)—Mo—S, and Mo—S—S angles of 156.3°, 82.9°, and 108.1°, respectively. The μ-disulfide unit is characterized by an average S—S distance of 2.144 Å, slightly longer than expected for a single bond, and a slightly puckered arrangement of S atoms; the S(1) and S(2) atoms lie −0.18(3) Å and 0.15(3) Å, respectively, out of the plane of the Mo and μ-O atoms. As expected, a lengthening of the Mo—N bonds trans to the terminal oxo ligands is observed. The structure and associated metrical parameters are analogous to those previously reported for the Tp* analogue by Roberts et al.[44]

Characterization of Molybdenyl Complexes. Microanalytical (Supporting Information) and mass spectrometric (Table 2) data for the molybdenyl complexes were in accord with the

(43) Xiao, Z.; Enemark, J. H.; Wedd, A. G.; Young, C. G. *Inorg. Chem.* **1994**, *33*, 3438−3441.
(44) Roberts, S. A.; Young, C. G.; Cleland, W. E., Jr.; Yamanouchi, K.; Ortega, R. B.; Enemark, J. H. *Inorg. Chem.* **1988**, *27*, 2647−2652.

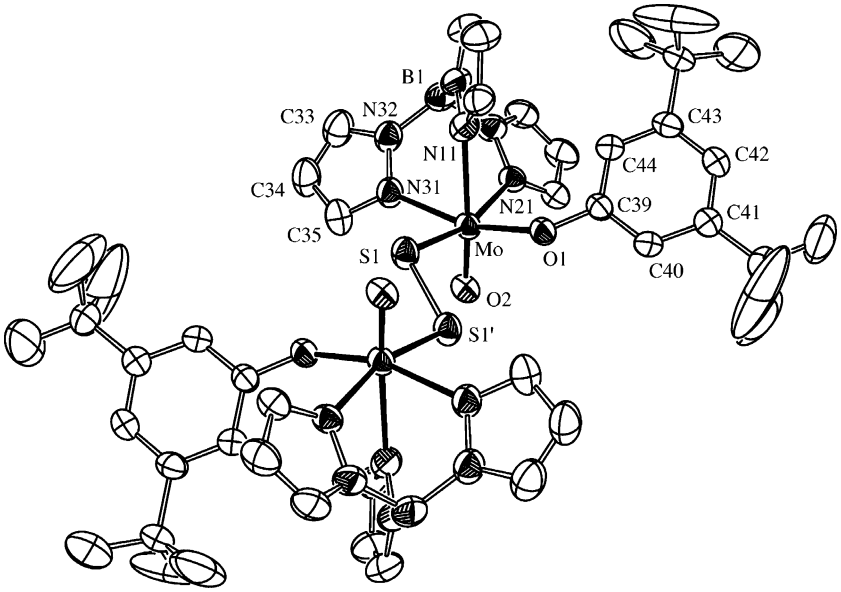

Figure 6. ORTEP projection of **5** drawn at the 30% probability level. Isopropyl groups and hydrogen atoms have been omitted for clarity.

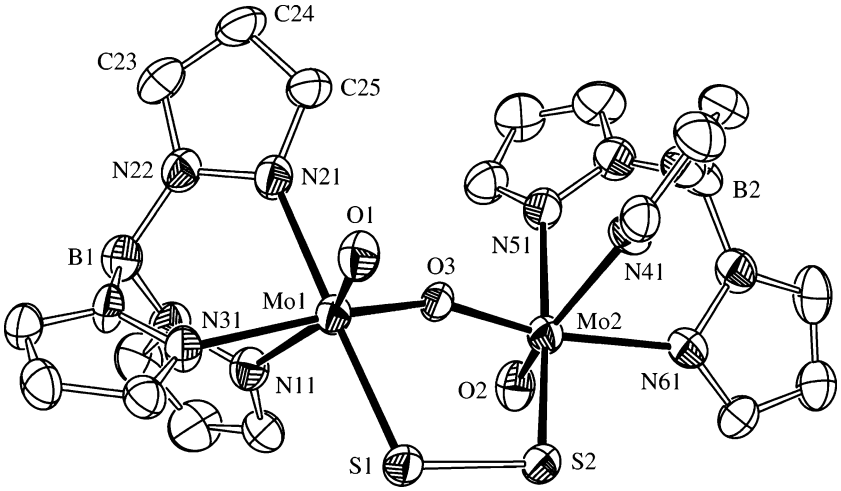

Figure 7. ORTEP projection of **8** at the 30% probability level. Isopropyl groups and hydrogen atoms have been omitted for clarity.

proposed formulations. Infrared spectra exhibited bands characteristic of the Tp^{iPr} ligand and a single terminal oxo ligand (ν(Mo═O) 942−933 cm^{-1}); the oxo stretches are at the low end of the range established for related molybdenyl complexes by Enemark and co-workers.[12,31] The complexes exhibited rhombic, frozen-glass EPR spectra consistent with molecular C_1 symmetry. The spectrum of **9** (Figure 8) was analogous to that of Tp*MoO(OSC_6H_4) reported earlier;[31] the remarkable similarity in g_i values is consistent with the observation by Enemark and co-workers that the EPR parameters for Tp^xMoO(L−L) species are dependent on the nature of the donor atoms rather than the chelate geometry.[45] The dominance of metal−ligand covalency on g_1 is also consistent with available data.[46]

Structure of Tp^{iPr}MoO($OSC_{10}H_6$). The coordination sphere of **11** (Figure 9) exhibits a distorted octahedral geometry and structural parameters consistent with those of related molybdenyl Tp* complexes.[12,31] The Mo−N(11) distance of 2.363(5) Å is significantly longer than those of Mo−N(21) and Mo−N(31) (2.195(6) and 2.211(6) Å, respectively) reflecting the strong

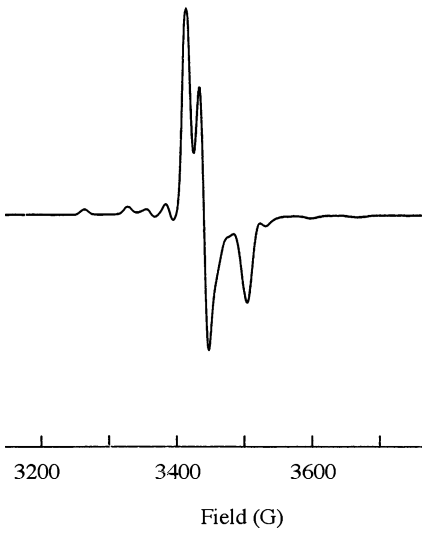

Figure 8. The frozen glass (toluene, 120 K) EPR spectrum of **9**.

(45) (a) Dhawan, I. K.; Pacheco, A.; Enemark, J. H. *J. Am. Chem. Soc.* **1994**, *116*, 7911−7912. (b) Dhawan, I. K.; Enemark, J. H. *Inorg. Chem.* **1996**, *35*, 4873−4882.

(46) Peariso, K.; Chohan, B. S.; Carrano, C. J.; Kirk, M. L. *Inorg. Chem.* **2003**, *42*, 6194−6203.

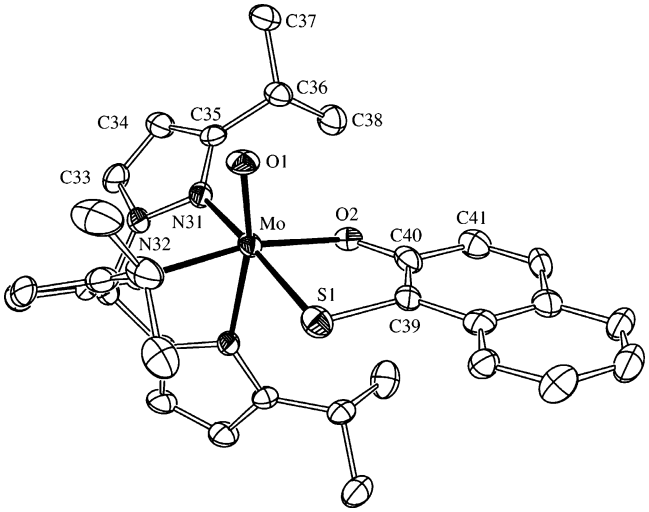

Figure 9. ORTEP projection of **11** at the 30% probability level with hydrogen atoms removed. The labeling of the pyrazole groups containing N(11) (trans to oxo) and N(21) follow that shown for the group containing N(31).

trans influence of the terminal oxo ligand. Each of the N−Mo−N bond angles are typically acute accounting for a major distortion from octahedral geometry. The Mo−O(1) and Mo−O(2) distances of 1.696(4) Å and 2.004(4) Å, respectively, are unremarkable, and the Mo−S(1) bond length of 2.388(2) Å lies within the expected range for a thiolate moiety.[42] The acute S(1)−Mo−O(2) bite angle of 81.18(13)° deviates significantly from ideal octahedral geometry. In structurally related Tp*MoO(bdt) (bdt = benzene-1,2-dithiolate), the S(1)−Mo−S(2) bite angle is marginally less acute at 85.12(6)°.[45] The molybdenum atom lies at the center of the distorted octahedron and is positioned 0.2187(24) Å above the mean plane comprising S(1), O(2), N(21), and N(31). The atoms S(1), O(2), C(39), and C(40) are almost coplanar (rms deviation 0.0123 Å) and form a fold angle of 13.06(26)° with the mean plane comprising atoms Mo, S(1), and O(2). Similar fold angles are observed for d^1 Tp*MoO(dithiolate) complexes, ranging from 6.9° to 21.3°.[47] The planarity and C−C bond lengths of the naphtholate coligand are consistent with an aromatic moiety (av. 1.40 Å). Molybdenum K-edge EXAFS studies were consistent with complexes **9** and **10** having first-coordination sphere structures exactly analogous to that of **11**, the parameters obtained being in excellent agreement with those determined for **11** by X-ray diffraction.[48]

Summary

An extended series of mononuclear oxosulfido-Mo(VI) complexes, Tp$^{i\text{Pr}}$MoOS(OAr), has been prepared and characterized. Complexes **1**−**3** are rare examples of *strictly* monomeric oxosulfido-Mo(VI) species that model key chemical and structural features of the oxidized active sites of Mo hydroxylases; the remaining complexes (**4**−**7**) are monomeric in solution but crystallize as dimeric species. Certain oxosulfido-Mo(VI) complexes undergo unprecedented aromatic C−H bond activation reactions leading to molybdenyl complexes bearing 2-mercaptophenolate or related naphtholate coligands. Oxosulfido-Mo(V) derivatives,[17] and Mo/Cu complexes such as Tp$^{i\text{Pr}}$MoO(OAr)(μ-S)Cu(Me$_3$tcn)[21] are also accessible. These complexes represent key milestones in our quest to develop Mo hydroxylase models that span relevant enzyme centers, oxidation states, and biomimetic reactions.

Understanding the reactivity of metalloproteins requires a detailed knowledge of the structural and electronic nature of the active site. The Tp$^{i\text{Pr}}$MoOS(OAr) complexes provide important insights into the reactivity and electronic structure[22] of the biologically unique *cis*-$[MoOS]^{2+}$ center in Mo hydroxylases. Spectroscopic and computational studies have shown that the frontier orbitals of the complexes, particularly the LUMO, possess significant sulfur character. In addition, the Mo═S unit is intimately involved in the chemical reactions of the complexes. This suggests that the current mechanistic proposals for xanthine oxidase may underestimate the role of the Mo═S unit during catalysis. The widely accepted interpretation implies that hydride transfer from substrate to Mo═*S* is associated with a concomitant nucleophilic attack of the C-8 carbon of xanthine by metal activated hydroxide. However, the terminal sulfur has the potential to play a more formal role in catalysis. For example, partial C-8···S bond formation may be involved in activating the C-8 carbon of xanthine for nucleophilic attack by the catalytically labile oxygen of xanthine oxidase. Ongoing work will focus on developing a comprehensive understanding of the chemical reactivity and electronic structure of the Tp$^{i\text{Pr}}$MoOS(OAr) derivatives and their Mo(V) counterparts. A detailed description of the bonding and chemistry of these model complexes should provide the foundation for a more informed and accurate understanding of the Mo hydroxylases.

Acknowledgment. We thank Mr. Craig Gourlay and Dr. Hugh H. Harris for experimental assistance and Dr. Gary D. Fallon, Monash University, for collecting the diffraction data for **11**. C.G.Y. gratefully acknowledges financial support from the Australian Nuclear Science and Technology Organization (for travel to SSRL), the Australian Research Council, and the donors of the Petroleum Research Fund administered by the American Chemical Society. G.N.G. acknowledges support from the Natural Sciences and Engineering Research Council, the Canadian Institutes for Health Research, the National Institutes of Health, and a Canada Research Chair award. SSRL is funded by the Department of Energy (DOE) BES, with further support by DOE OBER and the National Institutes of Health.

Supporting Information Available: Microanalytical and complete IR spectral data, the NMR spectrum of **1**, ORTEP projections of **2** and **3**, and crystallographic data in CIF format. This material is available free of charge via the Internet at http://pubs.acs.org.

JA056109U

(47) Joshi, H. K.; Cooney, J. J. A.; Inscore, F. E.; Gruhn, N. E.; Lichtenberger, D. L.; Enemark, J. H. *Proc. Natl. Acad. Sci. U.S.A.* **2003**, *100*, 3719−3724.

(48) Mo EXAFS spectra were recorded as described in: Hill, L. M. R.; George, G. N.; Duhme-Klair, A.-K.; Young, C. G. *J. Inorg. Biochem.* **2002**, *88*, 274−283. The number and type of backscattered atom, *R* (Å), and σ^2 (Å^2) values determined were as follows. For **9**: 1 Mo═O, 1.70, 0.0023(1); 1 Mo−O, 1.96, 0.0008(2); 1 Mo−S, 2.37, 0.0061(3); 3 Mo−N, 2.23, 0.0069(8). For **10**, 1 Mo═O, 1.70, 0.0020(1); 1 Mo−O, 1.93, 0.0029(3); 1 Mo−S, 2.37, 0.0030(2); 3 Mo−N, 2.19, 0.0117(8). For **11**, 1 Mo═O, 1.69, 0.0018(1); 1 Mo−O, 1.96, 0.0017(2); 1 Mo−S, 2.39, 0.0042(3); 3 Mo−N, 2.22, 0.0084(9).